Journal of Water Process Engineering 70 (2025) 106943

Contents lists available at ScienceDirect

Journal of Water Process Engineering

journal homepage: www.elsevier.com/locate/jwpe

Highly efficient recycled NH_2-MIL-53(Fe)/TiO_2/PVDF membrane for heterogeneous photo-Fenton degradation of tetracycline

Jia-Xin Song, Lei-Qin Sun, Shu-Ting Cheng, Xiao-Fang Shen, Yue-Hong Pang *

School of Food Science and Technology, Jiangnan University, Wuxi 214122, China

ARTICLE INFO

Editor: Laura Bulgariu

Keywords:
Tetracycline
NH_2-MIL-53(Fe)/TiO_2/PVDF
Membrane
Wastewater treatment
Heterogeneous photo-Fenton

ABSTRACT

Heterogeneous photo-Fenton catalysts play an important role in improving the efficiency of photo-Fenton reactions, but powder-form catalysts have caused pollution and difficulty in recovery to a certain extent. In this paper, NH_2-MIL-53(Fe) (MIL, Materials of Institut Lavoisier) and TiO_2, both possessing photocatalytic activity, were loaded onto polyvinylidene fluoride (PVDF) membranes with different compounding ratios by a simple vacuum filtration method to produce NH_2-MIL-53(Fe)/TiO_2/PVDF photocatalytic membranes. The prepared membranes were used to photo-Fenton degradation of organic pollutant tetracycline (TC) in wastewater. NH_2-MIL-53(Fe)/TiO_2/PVDF membrane demonstrated a highly efficient photo-Fenton degradation of TC (90.4 % within 60 min), and it can also achieve rapid recovery and good reusability (retained more than 80 % stable degradation efficiency after 5 consecutive uses). Active species trapping experiments confirmed the involvement of ·OH, h^+ and $^1O_2$ in the photo-Fenton degradation process, and ·OH radicals were the primary contributors. The degradation mechanism and possible reaction pathways were discussed. According to mass spectrometry results, TC formed eleven possible degradation intermediate products through three degradation pathways. The research provides an efficient and green method for treatment of antibiotic wastewater by designing environmental-friendly and rapid recovery of photocatalytic membranes, which is expected to be applied to the treatment of real wastewater samples.

1. Introduction

Antibiotics are a class of secondary metabolites that are synthesized by microorganisms, along with similar compounds that are chemically synthesized or semi-synthesized. They possess the capability to inhibit the development and existence of other microorganisms [1]. Over the past few decades, the application of antibiotics for the treatment of infections in both human beings and animals has increased dramatically due to climate change, population expansion, pollution, and rapid economic growth [2]. Tetracycline (TC) is considered a broad-spectrum antibiotic due to its low cost, low toxicity, and wide range of applications [3]. Due to the widespread use of TC, residues have been found in wastewater from both livestock and aquaculture [4]. It has been reported that about 210,000 t of TC wastewater are released into the aquatic ecological system annually in recent decade [1]. The direct discharge of untreated wastewater containing antibiotics can be harmful to water and soil, and may also remain in agricultural products through the ecological chain, causing food safety problems and presenting a threat to human health [5]. People may consume water contaminated with antibiotics, resulting in antibiotic resistance, imbalance of the intestinal flora, and other complications [6,7]. TC may induce oxidative stress, resulting in liver cell damage and causing membrane damage [8,9]. However, the tetracycline molecule contains a benzene ring and hetero cyclic rings, which makes it exhibit specific absorption peaks in both infrared spectroscopy and ultraviolet-visible spectroscopy and presents a challenge for its elimination in natural environments [10]. Consequently, it is crucial to establish an effective and economical approach for the removal of TC.

Physical, biological, and chemical methods are the most commonly utilized methods for treating wastewater containing organic pollutants [11]. Among the physical methods for the removal of organic pollutants in wastewater, the adsorption method is the most extensively applied [12]. Adsorption is effective in removing pollutants but does not degrade them [13]. The biodegradation approach utilizes the metabolic capacity of microorganisms to transform organic compounds in wastewater into inorganic materials, but cultivating these microorganisms can be complex and expensive [14]. Traditional chemical reduction and oxidation methods may produce large amounts of sludge during

---

* Corresponding author.
E-mail address: yhpang@jiangnan.edu.cn (Y.-H. Pang).

https://doi.org/10.1016/j.jwpe.2025.106943
Received 5 November 2024; Received in revised form 2 January 2025; Accepted 3 January 2025
Available online 9 January 2025

treatment [15]. During the recent years, advanced oxidation processes (AOPs) to produce ·OH are a powerful approach for addressing refractory organic contaminants [16]. The heterogeneous photo-Fenton procedure offers a series of advantages of high oxidizing capacity and simple operation, which is suitable for wastewater treatment [17–19]. The heterogeneous photo-Fenton process employs solid catalysts, rather than soluble Fe^{2+} or Fe^{3+}, which offers a broad pH response range and recyclable catalysts [20,21]. The use of photocatalysts greatly enhances the efficiency of photocatalytic degradation of pollutants [22–25]. Currently, there is still significant importance in developing heterogeneous photocatalysts with outstanding catalytic activity.

Fe-based metal-organic frameworks (Fe-MOFs) possess the advantages of high porosity, unoccupied metal sites, adjustable chemistry, easy synthesis, and environmental friendliness, while they are extensively utilized in the area of separation, drug delivery, and catalytic degradation [26]. Among them, Materials Institute Lavoisier frameworks (MILs) have gained widespread attention for their excellent stability and distinctive structural characteristics [27]. The NH_2-functionalization of MOF has emerged as a promising strategy to significantly enhance both the stability of MOFs and visible light responses [28]. Based on this, NH_2-MIL-53(Fe) has become an important component of composite photocatalysts in recent years and has been applied in the degradation of antibiotics such as TC [29], oxytetracycline [30], and sulfamethoxazole [31]. TiO_2 is one of the most prominent photocatalysts in semiconductors due to its excellent photocatalytic ability, chemical stability and cost-effectiveness [12]. Generally, the improvement of photocatalytic activity through the synergistic combination of different materials has been reported as an effective strategy [32,33]. On this basis, the development of catalysts with synergistic effects, stable light absorption performance, easy recycling, high activity and sustainable use is highly important for the photo-Fenton reaction. Polyvinylidene fluoride (PVDF) membranes are polymeric materials with nano pore size, heat and chemical resistance [34]. In recent years, the construction of functional composite membranes by immobilizing MOFs onto polymer substrates has attracted attention [35], and this combination enables the concurrent acquisition of the advantages offered by functional MOFs and malleable polymers, and improve the practical application value of the corresponding composites.

In this work, NH_2-MIL-53(Fe) served as a photocatalyst and complexed with TiO_2, which was deposited onto the surface of PVDF membranes through a simple vacuum filtration approach. A NH_2-MIL-53(Fe)/TiO_2/PVDF reaction membrane with different compounding ratios was prepared and utilized for photo-Fenton degradation of TC in wastewater. The practicability and stability of this membrane and the mechanism of TC degradation were explored, and a potential pathway for its degradation was further proposed. This research offers insights into designing green and rapidly recyclable photocatalytic membranes for the efficient degradation of TC.

2. Materials and methods

2.1. Chemicals and reagents

The specifics regarding the chemicals and reagents can be found in Text S1.

2.2. Preparation of NH_2-MIL-53(Fe)/TiO_2/PVDF membrane

Firstly, NH_2-MIL-53(Fe) was synthesized using a solvothermal approach [36]. In short, equal molar amounts of $FeCl_3 \cdot 6H_2O$ and 2-aminoterephthalic acid (NH_2-H_2BDC) were dissolved in 36 mL of DMF and stirred for 30 min to prepare the solution. The mixed solution was subjected to solvothermal treatment at 150 °C for 24 h. After cooling, the product was washed three times with DMF and methanol. The final product was dried at 60 °C. Then, the complexed NH_2-MIL-53(Fe)/TiO_2 materials were prepared. The mixtures of NH_2-MIL-53(Fe) and TiO_2 in different mass ratios (1:1; 1:2; 2:1) were dispersed in ultrapure water and sonicated for 60 min at room temperature to make them well mixed.

The procedure for preparing NH_2-MIL-53(Fe)/TiO_2/PVDF membranes was as follows: (1) The pretreatment process of PVDF membranes followed previous report [37]. The pristine PVDF membranes were soaked in anhydrous ethanol for 2 h to remove the adherents located on the surface of the membrane, and then they were dipped into ultrapure water and soaked for 12 h to wash away the residual ethanol solution. At last, the treated PVDF membrane was dried at room temperature. (2) NH_2-MIL-53(Fe)/TiO_2/PVDF membranes were prepared by vacuum filtration method [38]. The aqueous solution of NH_2-MIL-53(Fe)/TiO_2 was filtered on a PVDF membrane through a vacuum filtration device, the amount of NH_2-MIL-53(Fe)/TiO_2 (1:1, 1:2, 2:1) loaded on the PVDF membrane were 7.5 mg/7.5 mg, 5 mg/10 mg, 10 mg/5 mg, respectively. At the same time, 5 mL of PEG and 5 mL of GA (25 % aqueous solution) were successively pumped and filtered on the membrane to be used as a crosslinking agent. Finally, the prepared complex photocatalytic membrane was dried at room temperature. Similarly, NH_2-MIL-53(Fe)/PVDF and TiO_2/PVDF membranes can be prepared using the similar way.

2.3. Characterization

Further details concerning the characterization can be found in **Text S2**.

2.4. Heterogeneous photo-Fenton degradation of TC in aqueous solution

The degradation performance of the photocatalytic membranes was assessed according to the efficiency of Fenton degradation of TC under visible light irradiation (500 W Xe-lamp). In a multi-position photochemical reactor (HF-GHX-VII, Shanghai Hefan Co., China), the xenon lamp is located at the center of the reactor and is equipped with circulating water to ensure room temperature. Meanwhile, the quartz test tubes are placed parallel to the xenon light source at a distance of 10 cm, the average intensity value measured using digital optical power and energy meter was 48.57 $mW \cdot cm^{-2}$.

The prepared 1/2 photocatalytic membrane was added to a 30 mg/L TC solution and stirred under dark conditions for 30 min to achieve the adsorption-desorption equilibrium. Then a certain amount of H_2O_2 was added to the reaction system and a xenon lamp was turned on at the same time. During the photo-Fenton reaction, 1 mL of the solution was taken at regular intervals and subsequently filtered through a 0.22 μm filter tip. Finally, the concentration of TC was measured at 357 nm through UV spectrophotometry. The degradation efficiency of TC through photo-Fenton process was calculated according to Eq. (1).

$$\eta\ (\%) = \frac{(C_0 - C_t)}{C_0} \times 100\% \tag{1}$$

In the above Eq. (1), C_0 represents the initial concentration of TC, while C_t is the concentration of TC measured at the sampling time t (min).

In addition to investigating the impact of pH and real water samples on TC degradation, the initial pH of the TC solution in other degradation experiments was around 5.0. For the free radical capture experiment, the used trapping agents were tert-butanol (TBA, 10 mmol/L), furfuryl alcohol (FFA, 10 mmol/L) and formic acid (FA, 10 mmol/L).

The preparation process and photo-Fenton reaction process of NH_2-MIL-53(Fe)/PVDF membrane are illustrated in Fig. 1.

3. Results and discussion

3.1. Characterization

The physical images of the prepared photo-Fenton reaction membrane were illustrated in Fig. 2a-f. The blank PVDF membrane (a) appeared white. When TiO_2 was loaded, the color became brighter milky

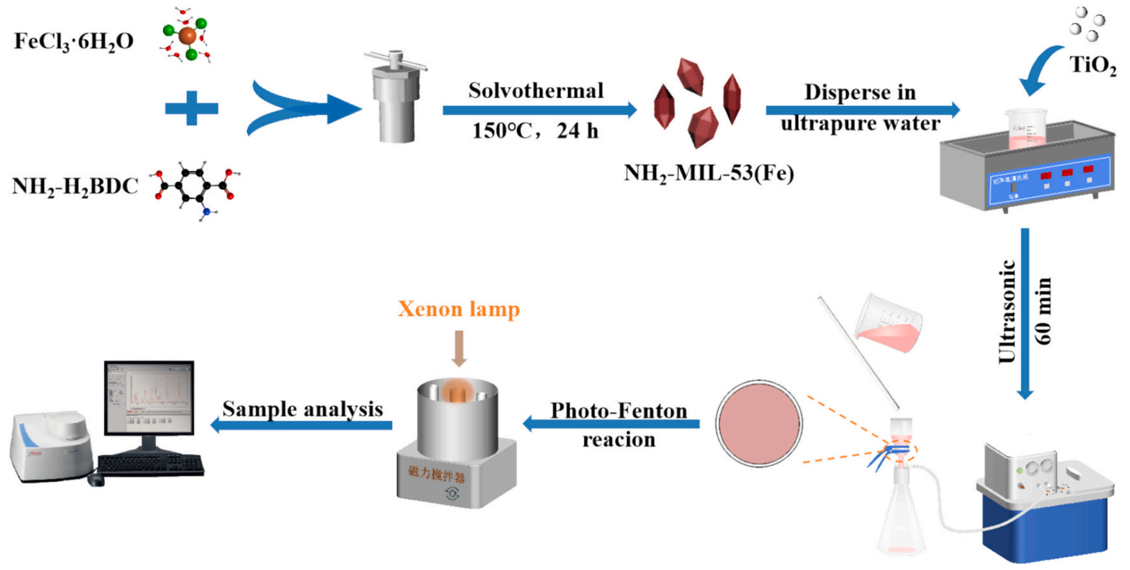

Fig. 1. Schematic illustrations of preparation process and photo-Fenton reaction process of NH_2-MIL-53(Fe)/PVDF membrane.

white (b); When NH_2-MIL-53(Fe) material was loaded, the color of the membrane became brick red (c); When NH_2-MIL-53(Fe) and TiO_2 were loaded with different proportions, the color of the membrane gradually deepened along with the rise of the proportion of NH_2-MIL-53(Fe)/TiO_2. When NH_2-MIL-53(Fe)/TiO_2 (1:1) was loaded, the color of the membrane was brick purple (d). At NH_2-MIL-53(Fe)/TiO_2 (1:2), the color of the membrane was mainly purple to white (e). At NH_2-MIL-53(Fe)/TiO_2 (2:1), the color of the membrane appeared as brick red to purple (f). The morphology of the prepared membrane was smooth, and the loaded materials were uniformly distributed.

The SEM images of NH_2-MIL-53(Fe)/TiO_2 and NH_2-MIL-53(Fe)/TiO_2/PVDF were presented in Fig. 2g-h. The powdered NH_2-MIL-53 (Fe)/TiO_2 material appeared to have a mixed structure of spindle and sphere, with NH_2-MIL-53(Fe) presenting a spindle type and TiO_2 presenting a sphere type, and TiO_2 aggregated on the surface of NH_2-MIL-53 (Fe). The energy dispersive X-ray spectroscopy (EDX) elemental mappings of NH_2-MIL-53(Fe)/TiO_2 showed the uniform distribution of Ti element on the spindle (**Fig. S1**). The mixed materials compounded on the PVDF membrane exhibited a homogeneous distribution on the surface of the membrane, and because of the large proportion of NH_2-MIL-53(Fe), the overall appearance of the spindle configuration, and the spherical structure of TiO_2 was dispersed in the surrounding area (**Fig. 2i-j**). The presence of C, O, N, F, Ti, and Fe in the NH_2-MIL-53(Fe)/TiO_2/PVDF membrane was confirmed through the EDX elemental images in **Fig. S2**, and the uniform distribution of elements further confirms the uniform distribution of mixed materials on the membrane surface.

The XRD patterns for the material and membranes obtained are showed in Fig. 2k-l. The characteristic diffraction peaks of the PVDF membrane alone appeared at 17.9°, 20.4°, 23.0° and 26.2°. When the material was loaded on the PVDF membrane, the diffraction peaks of NH_2-MIL-53(Fe)/PVDF appeared at 9.4°, 10.8°, 18.2°, which was in accordance with those reported in the literature [39]. The diffraction peaks of TiO_2/PVDF at 25.8°, 38.4°, 48.5° are attributed to the (101), (004), and (200) planes, which was consistent with the previous report [40]. In addition, the characteristic diffraction peaks of NH_2-MIL-53 (Fe)/TiO_2/PVDF (2:1) at 18.0°, 20.1°, 22.9°, and 25.7° corresponded to the blank PVDF membrane, and the peaks at 9.1°, 10.7°, 38.2°, and 48.4° indicated the presence of NH_2-MIL-53(Fe) and TiO_2 (Fig. 2k). In Fig. 2l, the diffraction peaks of NH_2-MIL-53(Fe)/TiO_2/PVDF (2:1) at 7.3°, 9.1°, 18.0°, 20.1°, 22.9°, 25.7°, 38.1°, 48.4°, 54.2°, 55.5° and 63.2° corresponded to the powder material, and the XRD major diffraction peaks of the PVDF membranes loaded with the material were essentially in agreement with those of the powdered form, indicating successful loading of the material onto the PVDF membrane.

The elemental compositions and valence states of the surface of NH_2-MIL-53(Fe)/TiO_2/PVDF and NH_2-MIL-53(Fe)/TiO_2 were analyzed by X-ray photoelectron spectroscopy (XPS), and the results are presented in Fig. 3. NH_2-MIL-53(Fe)/TiO_2 and NH_2-MIL-53(Fe)/TiO_2/PVDF was mainly composed of C, N, O, Fe and Ti elements, and the XPS spectrum of NH_2-MIL-53(Fe)/TiO_2/PVDF was almost the same as that of NH_2-MIL-53(Fe)/TiO_2 (Fig. 3a), indicating the element composition and valence state of NH_2-MIL-53(Fe)/TiO_2 had not changed after being loaded on the PVDF membrane. The high-resolution C 1s spectrum demonstrated three characteristic peaks at 284.8, 286.0 and 288.2 eV (Fig. 3b), which corresponded to C—C, C—N and C—O. The peaks of N 1 s at 399.0, 400.4 eV can be attributed to C—N and N—H (Fig. 3c). The O 1 s peak can be divided into three peaks at 529.7, 531.5 and 532.6 eV (Fig. 3d), corresponding to the Ti—O bonds of TiO_2, the oxygen atoms on the H_2BDC linkers (C=O) and the Fe—O bonds of NH_2-MIL-53(Fe) [41], respectively. In Fig. 3e, Fe 2p peaks at 714.2 and 726.8 eV corresponded to Fe $2p_{3/2}$ and Fe $2p_{1/2}$, and peaks at 710.4 and 724.3 eV were attributed to Fe(III) and Fe—O bond, which also confirmed the existence of iron oxide clusters [42]. The Ti 2p peaks at 458.3 and 464 eV showed the presence of Ti $2p_{3/2}$ and Ti $2p_{1/2}$, corresponding to Ti^{4+} in TiO_2 (Fig. 3f) [43]. These further proved the successful loading of composite material on the PVDF membrane.

3.2. *Photo-Fenton degradation performance*

3.2.1. *TC degradation activity by different ratios of reaction membranes*

Photo-Fenton-degradation performance studies of the prepared NH_2-MIL-53(Fe)/TiO_2/PVDF membranes were carried out under H_2O_2 and visible light with TC as a model target (Fig. 4). When five different ratios of membranes degraded TC, the degradation rate increased the most in the first 15 min, which may be imputed to the phenomenon that TC adsorbed on the surface of the material will react rapidly when it is just contacted with H_2O_2 and light, and as the reaction proceeds, TC intermediates are generated, and the active species react with TC on the one hand, and de-activate the intermediates generated by TC on the other hand, and thus the reaction will gradually slow down. As shown in Fig. 4a, both the NH_2-MIL-53(Fe)/PVDF membrane and the TiO_2/PVDF membrane had a certain degradation effect on TC within 60 min, with degradation rates of 58.4 % and 44.4 %, respectively. The degradation

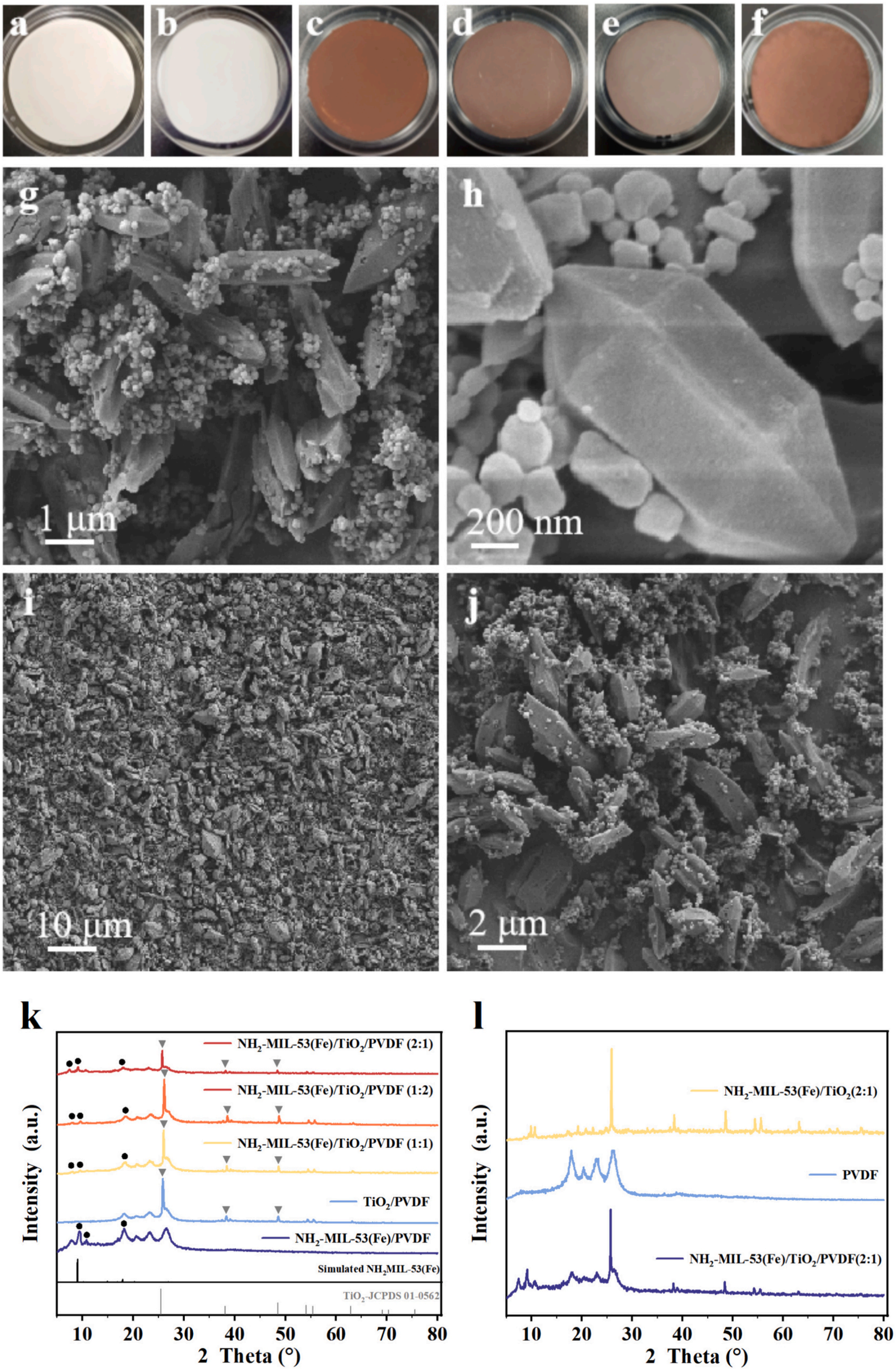

Fig. 2. Physical image of (a) PVDF, (b) TiO_2/PVDF, (c) NH_2-MIL-53(Fe)/PVDF membrane, NH_2-MIL-53(Fe) and TiO_2 composite membrane with different compounding ratio of (d) (1:1), (e) (1:2), (f) (2:1); SEM images of powdered material (g) and (h), NH_2-MIL-53(Fe)/TiO_2/PVDF (i) and (j) in membrane form; XRD patterns of (k) NH_2-MIL-53(Fe)/PVDF, TiO_2/PVDF, NH_2-MIL-53(Fe) and TiO_2 composite membrane with different compounding ratio of (1:1), (1:2), (2:1) and (l) NH_2-MIL-53 (Fe)/TiO_2/PVDF membrane (2:1), PVDF membrane and NH_2-MIL-53(Fe)/TiO_2 powder.

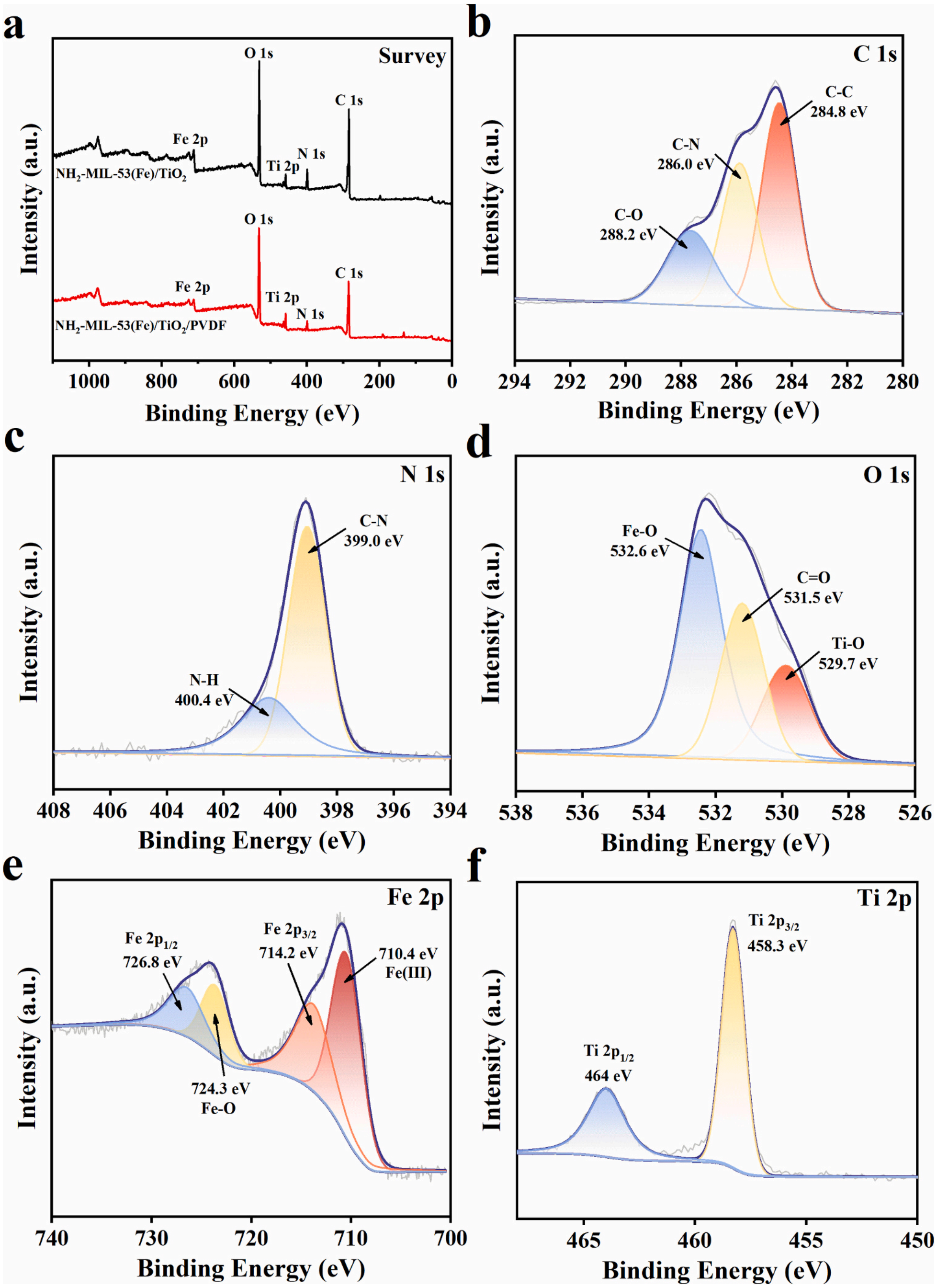

Fig. 3. (a) XPS survey spectra of NH_2-MIL-53(Fe)/TiO_2 and NH_2-MIL-53(Fe)/TiO_2/PVDF, high-resolution XPS spectra of NH_2-MIL-53(Fe)/TiO_2/PVDF: (b) C 1 s, (c) N 1 s, (d) O 1 s, (e) Fe 2p, (f) Ti 2p.

rates of three different compounding ratios (1:1; 1:2; 2:1) of NH_2-MIL-53 (Fe)/TiO_2/PVDF membranes were 86.4 %, 85.4 %, and 90.4 %, respectively. The degradation rates of TC were significantly improved when the materials were compounded, indicating a synergistic interaction between NH_2-MIL-53(Fe) and TiO_2.

In addition, the TC degradation process was subjected to further investigation by proposed zero-order, first-order and second-order kinetic models (**Table 1** and Fig. 4b-d). Through the comparison of the correlation coefficient (R^2) values of the proposed three kinetic models, the proposed second-order kinetic model is superior to the other two in terms of describing the TC photo-Fenton degradation process. Subsequent experimental investigations have used the proposed second-order kinetic model to represent the photo-Fenton degradation rate profile of TC. The constant for the degradation rate of NH_2-MIL-53(Fe)/TiO_2/PVDF membrane at three different compounding ratios (2:1; 1:1; 1:2) were 0.0041 min^{-1}, 0.0036 min^{-1} and 0.0033 min^{-1}. Among them, NH_2-MIL-53(Fe)/TiO_2/PVDF membrane (2:1) was the highest. Based on the above results, the subsequent experimental investigations were conducted using PVDF membranes with a blending ratio of 2:1.

3.2.2. *TC degradation activity in different systems*

Fig. 5 illustrates the degradation effect of NH_2-MIL-53(Fe)/TiO_2/PVDF membranes on TC under different reaction systems. As is depicted in Fig. 5a, the degradation rate of TC in the system composed of NH_2-MIL-53(Fe)/TiO_2/PVDF and H_2O_2 was 42.6 % in 60 min, which indicated that the photocatalytic membrane prepared under the condition of no light could also react with H_2O_2 to a certain extent. The pure adsorption of NH_2-MIL-53(Fe)/TiO_2/PVDF on TC could reach about

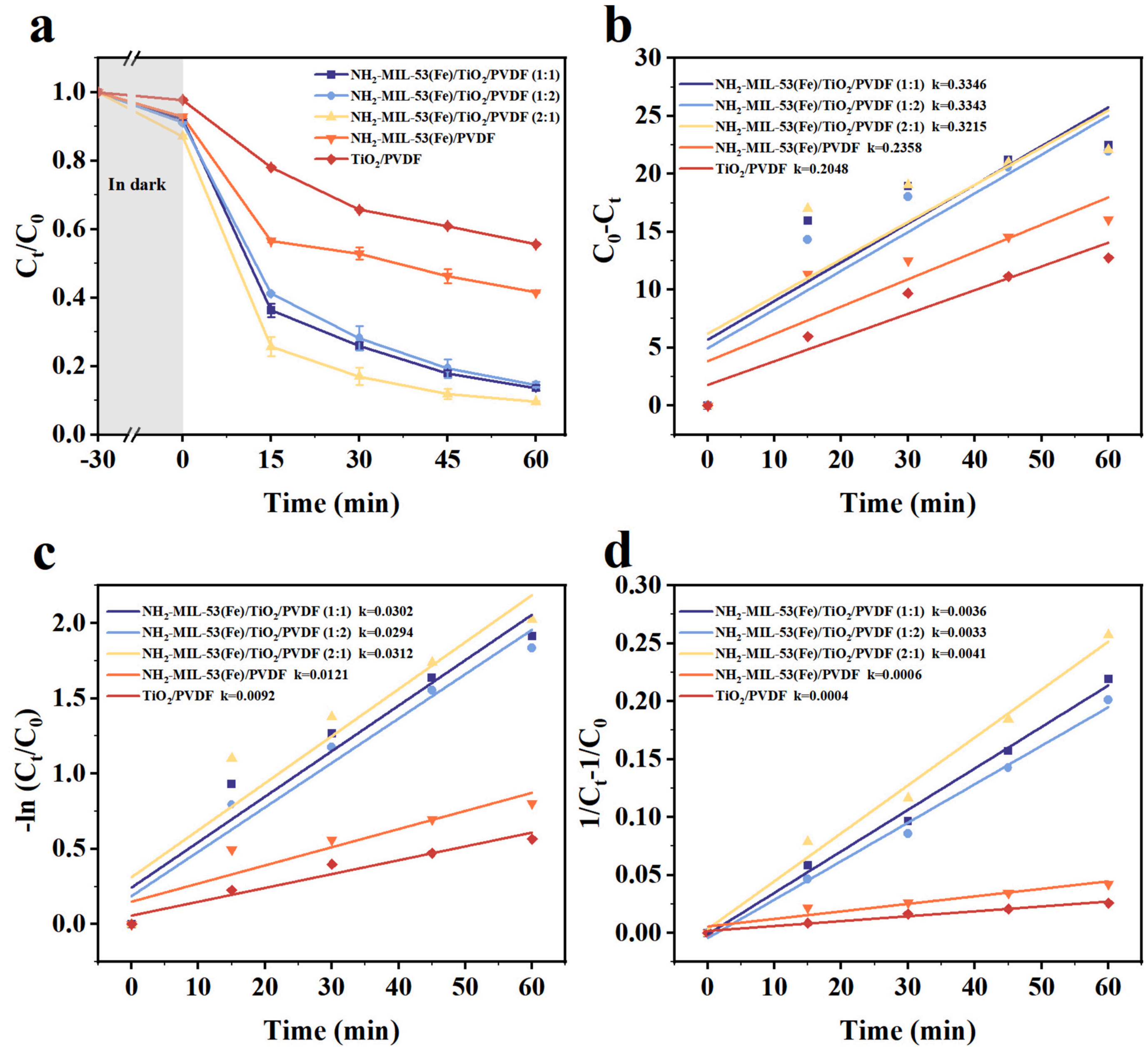

Fig. 4. (a) The photo-Fenton degradation curves of TC by NH_2-MIL-53(Fe)/TiO_2/PVDF membranes with different complex ratios, (b) the corresponding zero-order kinetic fitting curves, (c) first-order kinetic fitting curves, (d) second-order kinetic fitting curves.

Table 1
Kinetic rate constants for the degradation of TC by different catalysts.

Catalysts	Reaction condition	Zero-order C_0-$C_t = k_0t$		First-order -ln $(C_t/C_0) = k_1t$		Second-order $1/C_t$-$1/C_0 = k_2t$	
		K_0	R^2	K_1	R^2	K_2	R^2
NH_2-MIL-53(Fe)/PVDF	+ H_2O_2 + light	0.2358	0.6972	0.0121	0.8032	0.0006	0.8952
TiO_2/PVDF	+ H_2O_2 + light	0.2048	0.8803	0.0092	0.9315	0.0004	0.9690
NH_2-MIL-53(Fe)/TiO_2/PVDF (1:1)	+ H_2O_2 + light	0.3346	0.6745	0.0302	0.9097	0.0036	0.9924
NH_2-MIL-53(Fe)/TiO_2/PVDF (1:2)	+ H_2O_2 + light	0.3343	0.7341	0.0294	0.9416	0.0033	0.9916
NH_2-MIL-53(Fe)/TiO_2/PVDF (2:1)	+ H_2O_2 + light	0.3215	0.6095	0.0312	0.8660	0.0041	0.9870

11.3 %, and when both visible light and NH_2-MIL-53(Fe)/TiO_2/PVDF were concurrently present, the photocatalysis could degrade about 17.8 % of the TC, and the degradation rate of the TC compared with that of other systems was significantly enhanced when NH_2-MIL-53(Fe)/TiO_2/PVDF, H_2O_2 and visible light were present simultaneously, reaching 88.2 %. This result indicated that H_2O_2, visible light and the catalyst exhibit a synergistic effect. Visible light irradiation triggered the photo-Fenton reaction, which improved the cyclic conversion of Fe(III)/Fe(II) via the transfer of photogenerated electron-hole, thus promoting the photo-Fenton reaction. Fig. 5b shows the proposed secondary kinetic

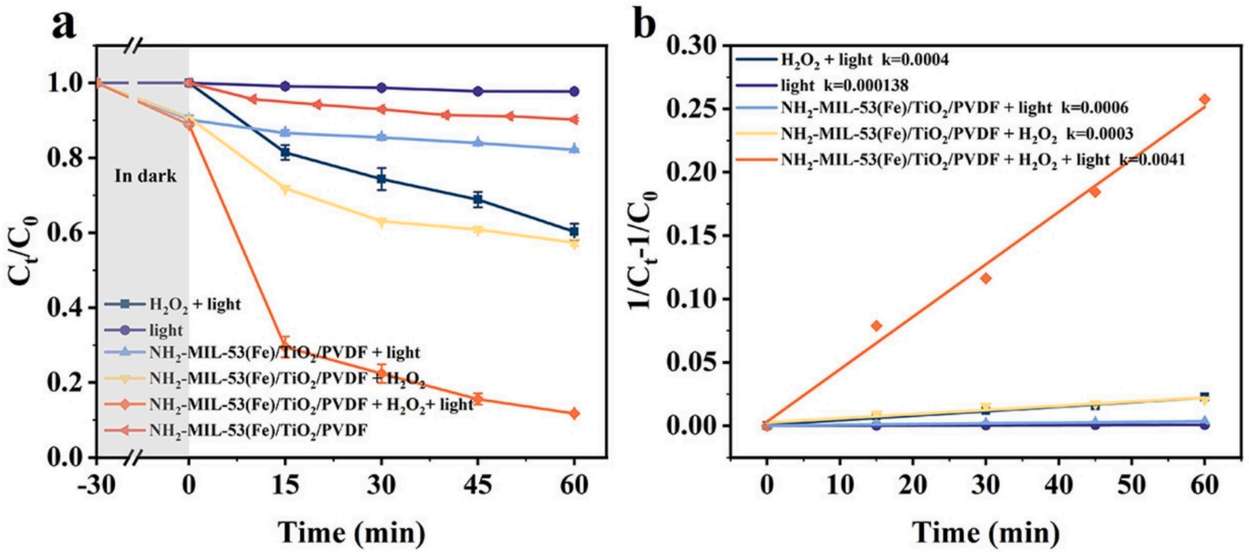

Fig. 5. (a) The photo-Fenton degradation curves of TC under different reaction systems (b) the corresponding second-order kinetic fitting curves of different systems.

rate curves for the degradation of TC in different reaction systems, and the kinetic rate constant of the NH_2-MIL-53(Fe)/TiO_2/PVDF + H_2O_2 + light system was 0.0041 min^{-1}, which was higher than that of NH_2-MIL-53(Fe)/TiO_2/PVDF + light (0.0006 min^{-1}), NH_2-MIL-53(Fe)/TiO_2/PVDF + H_2O_2 (0.0003 min^{-1}) and H_2O_2 + light (0.0004 min^{-1}). This indicated that the best degradation rate of TC was achieved under the photo-Fenton reaction system.

3.2.3. Influence factors on TC degradation

To determine the optimal conditions for the photo-Fenton reaction of NH_2-MIL-53(Fe)/TiO_2/PVDF membranes, the influence of each parameter on the reaction was investigated.

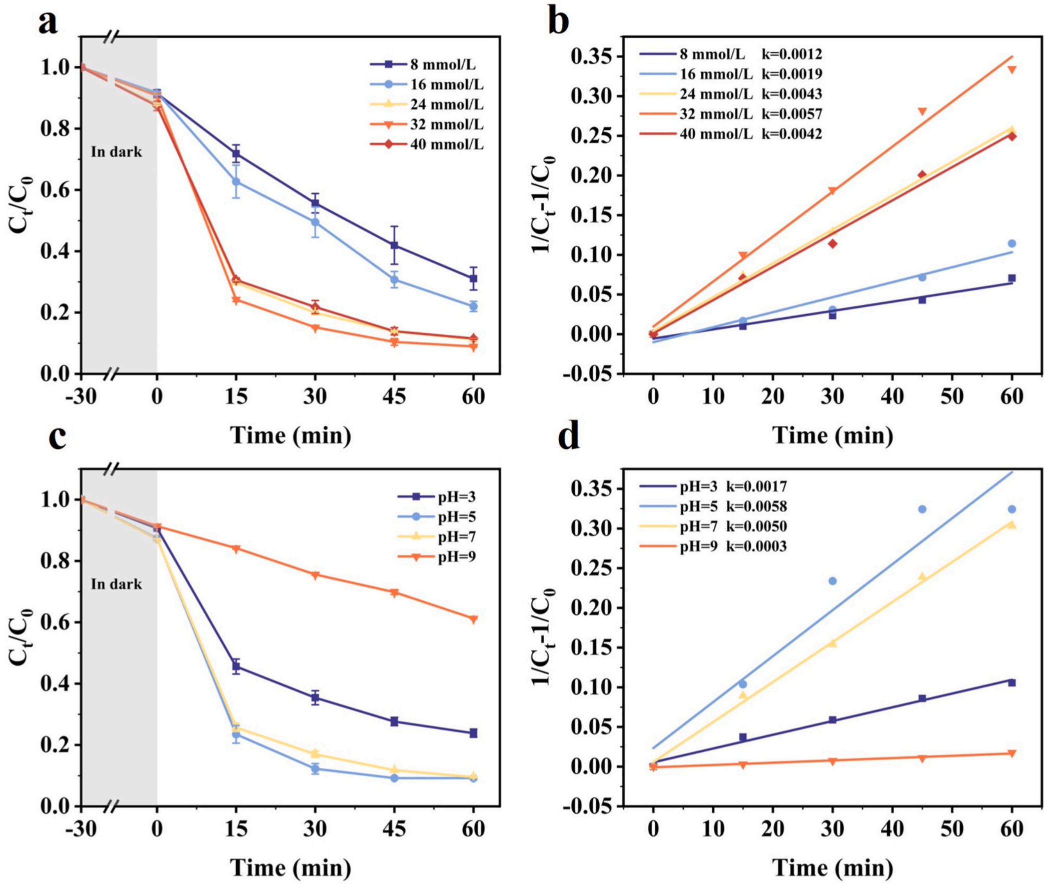

Fig. 6. (a) The photo-Fenton degradation curves of TC by NH_2-MIL-53(Fe)/TiO_2/PVDF membrane under different H_2O_2 concentrations and (b) the corresponding second-second kinetic fitting curves (c) The photo-Fenton degradation curves of TC by NH_2-MIL-53(Fe)/TiO_2/PVDF membrane under different pH conditions and (d) the corresponding second-order kinetic fitting curves.

Firstly, the effect of H_2O_2 concentration on the photo-Fenton degradation of TC was explored to clarify the optimal concentration of H_2O_2. The results were illustrated in Fig. 6a-b. When the concentration of H_2O_2 was raised from 8 mmol/L to 24 mmol/L, the degradation rate of TC rose from 68.9 % to 88.7 %, and the associated secondary kinetic rate constant increased from 0.0012 min^{-1} to 0.0043 min^{-1} due to the fact that an increase in H_2O_2 concentration resulted in a higher production of ·OH. However, when the H_2O_2 concentration was further increased to 40 mmol/L, the related secondary kinetic rate constant exhibited a pattern of initially increasing followed by a decrease, from 0.0043 min^{-1} to 0.0057 min^{-1} and subsequently to 0.0042 min^{-1}, whereas the corresponding TC degradation rate remained basically invariant. This phenomenon may be accounted to the reaction of excessive H_2O_2 with ·OH, resulting in the formation of HO_2·, which has low reactivity [44]. As a result, there was a reduction in the amount of ·OH, and the degradation rate showed insignificant changes. The optimal concentration of H_2O_2 was very significant for cost control, and the concentration of H_2O_2 was finally selected to be 24 mmol/L in combination with the degradation effect and considering the subsequent application in practice.

The initial pH of the solution was modified through the utilization of 0.1 mol/L H_2SO_4 or NaOH to investigate the effect of pH on the process of TC degradation, as illustrated in Fig. 6c-d. As the pH level rises, the degradation rate of TC initially rose, but then it decreased afterward. The degradation rate of TC was 76.1 % at pH = 3.0, and with the increase of pH, it reached the maximum value within 60 min at pH = 5.0–7.0, and decreased to 38.7 % when the initial pH was elevated to 9.0. The pH of the solution affected the surface charge of the catalyst, thereby impacting its interaction with the target [45].

Fig. S3 showed the zeta potential of NH_2-MIL-53(Fe)/TiO_2 composite at pH = 3.0–9.0. It was observed that the zeta potential of the NH_2-MIL-53(Fe)/TiO_2 complex diminished as pH increased, and its zero-point charge was 4.3. When the pH of the solution was less than 4.3, the NH_2-MIL-53(Fe)/TiO_2 complex was positively charged; and vice versa. TC molecules were usually present in three forms [45]: TC^+ at pH levels below 3.3, TC^0 between pH 3.3 and 7.7, and TC^- or TC^{2-} when the pH exceeds 7.7. When the pH of the solution was adjusted to 3, the TC predominantly existed as TC^+, and the surface of the NH_2-MIL-53(Fe)/TiO_2 composite material was positively charged. Due to the same kind of charge, repulsive forces between the target and the catalyst would obstruct the adsorption of TC onto the catalyst surface, resulting in a reduced rate of photo-Fenton degradation. When the initial pH of the solution ranged from 5.0 to 7.0, TC primarily existed as TC^0, with a portion existing as TC^-. At this time, the surface of the catalyst exhibited a negative charge, leading to weakened repulsion between TC and the catalyst. According to the above results, it could be inferred that the adsorption of TC onto the catalyst surface in the range of pH = 5.0–7.0 may mainly depend on intermolecular van der Waals forces. Finally, upon attaining a pH value of 9.0 for the solution, TC existed mainly in the form of TC^- and TC^{2-}, and since both catalyst and target TC were negatively charged, mutual repulsion occurs, which likewise inhibited the adsorption of TC onto the catalyst surface, resulting in a more pronounced reduction in the photo-Fenton degradation rate. Additionally, under alkaline conditions, the contact between H_2O_2 and the reactive active sites would also be hindered, leading to a decrease in ·OH generation and consequently lowering the degradation rate of TC. The degradation rates of TC were above 76.0 % in the pH range of 3.0–7.0, illustrating that the reaction system exhibited a broad pH response. Considering that the wastewater was generally acidic, pH = 5.0 was chosen for subsequent experiments to investigate.

In actual aqueous environments, the coexistence of inorganic anions may affect the degradation [46]. To investigate the capability of the photo-Fenton system dominated by NH_2-MIL-53(Fe)/TiO_2/PVDF membranes for the degradation of organic pollutants in real-world applications, simulated wastewater samples were created by dissolving an aqueous solution containing various inorganic anions (Cl^-, $H_2PO_4^-$, and HCO_3^-) in a TC solution. As shown in Fig. 7a, where Cl^-, $H_2PO_4^-$ and HCO_3^- influenced the degradation of TC. The addition of Cl^-, $H_2PO_4^-$ and HCO_3^- resulted in a decrease in the degradation rate of TC by 7.0 %, 7.1 % and 3.8 %, respectively. This may be attributed to the capacity of Cl^-, $H_2PO_4^-$ and HCO_3^- to capture h^+ and ·OH, leading to the formation of weaker reactive radicals [47], which brought about a certain degree of reduction in the degradation rate of TC. However, in general, the degradation rate of TC could still exceed 80 % even with the addition of these inorganic anions, which indicates that the NH_2-MIL-53(Fe)/TiO_2/PVDF membrane had the potential to be applied in actual wastewater treatment.

The capability of the NH_2-MIL-53(Fe)/TiO_2/PVDF + H_2O_2 + light system in practical water treatment was assessed by examining its degradation impact on TC in both tap water and lake water. Lake water samples were sourced from Taihu Lake in Wuxi, China, while tap water was taken from the laboratory at Jiangnan University. Fig. 7b shows that the degradation rate of TC was comparable to the control when both tap water and lake water were used. The degradation rates of TC in simulated polluted water samples of both lake water and tap water were around 90.0 %, which indicated that the NH_2-MIL-53(Fe)/TiO_2/PVDF + H_2O_2 + light system possesses prospective application potential in actual wastewater treatment.

3.2.4. *Reusability and stability*

The stability and recyclability of the NH_2-MIL-53(Fe)/TiO_2/PVDF membranes are of great importance in practical applications. Their stability and recyclability were assessed via TC degradation cycling assays. The degradation rate of the membrane was 90.4 %, the high catalytic ability is due to the synergistic effect of NH_2-MIL-53(Fe) and TiO_2. After five cycles, the degradation rate still maintained over 80.0 % (Fig. 7c), indicating that the membrane used has excellent stability and recyclability. As depicted in Fig. 7d, the XRD spectra of NH_2-MIL-53(Fe)/TiO_2/PVDF membranes remain similar both prior to and following the photo-Fenton reaction, further proving that the catalyst used has good stability. In addition, **Fig. S4** showed the leached iron concentration during the photo-Fenton reaction, with leaching concentrations of 0.136 mg/L and 0.238 mg/L at 30 min and 60 min, respectively, which were much lower than the environmental standard of the European Union (2 mg/L) [48].

The catalyst loaded on the PVDF membrane did not show significant detachment after five cycles (**Fig. S5**). Compared with catalyst modified membranes reported in previous literature (**Table S2**), NH_2-MIL-53(Fe)/TiO_2/PVDF membrane had higher TC removal efficiency and better stability and reusability, thereby making wastewater treatment more environmentally friendly.

3.3. *Degradation mechanism*

3.3.1. *Identification of active species*

For the purpose of attaining a deeper understanding of the photo-Fenton reaction mechanism, experiments for trapping active species were conducted. FFA, FA and TBA served as scavengers for three active species, namely $^1O_2$, h^+ and ·OH. As depicted in Fig. 8, the degradation rates of TC decreased to different degrees after introducing different scavengers, respectively. Among them, the introduction of the TBA scavenger led to the most significant decrease in the degradation rate of TC, from 90.4 % to 57.4 %. Following the addition of FFA and FA scavengers, the degradation rates of TC dropped to 83.2 % and 76.2 %, and the above results indicated that the role of ·OH is crucial in the photo-Fenton-degradation reaction system of TC by NH_2-MIL-53(Fe)/TiO_2/PVDF + H_2O_2 + light, followed by h^+ and $^1O_2$.

3.3.2. *The degradation pathway of TC*

To further explore the degradation pathway of tetracycline, possible intermediates of TC were examined using mass spectrometry (MS) (**Fig. S6** and **Table S1**), and Fig. 9 illustrates three potential degradation

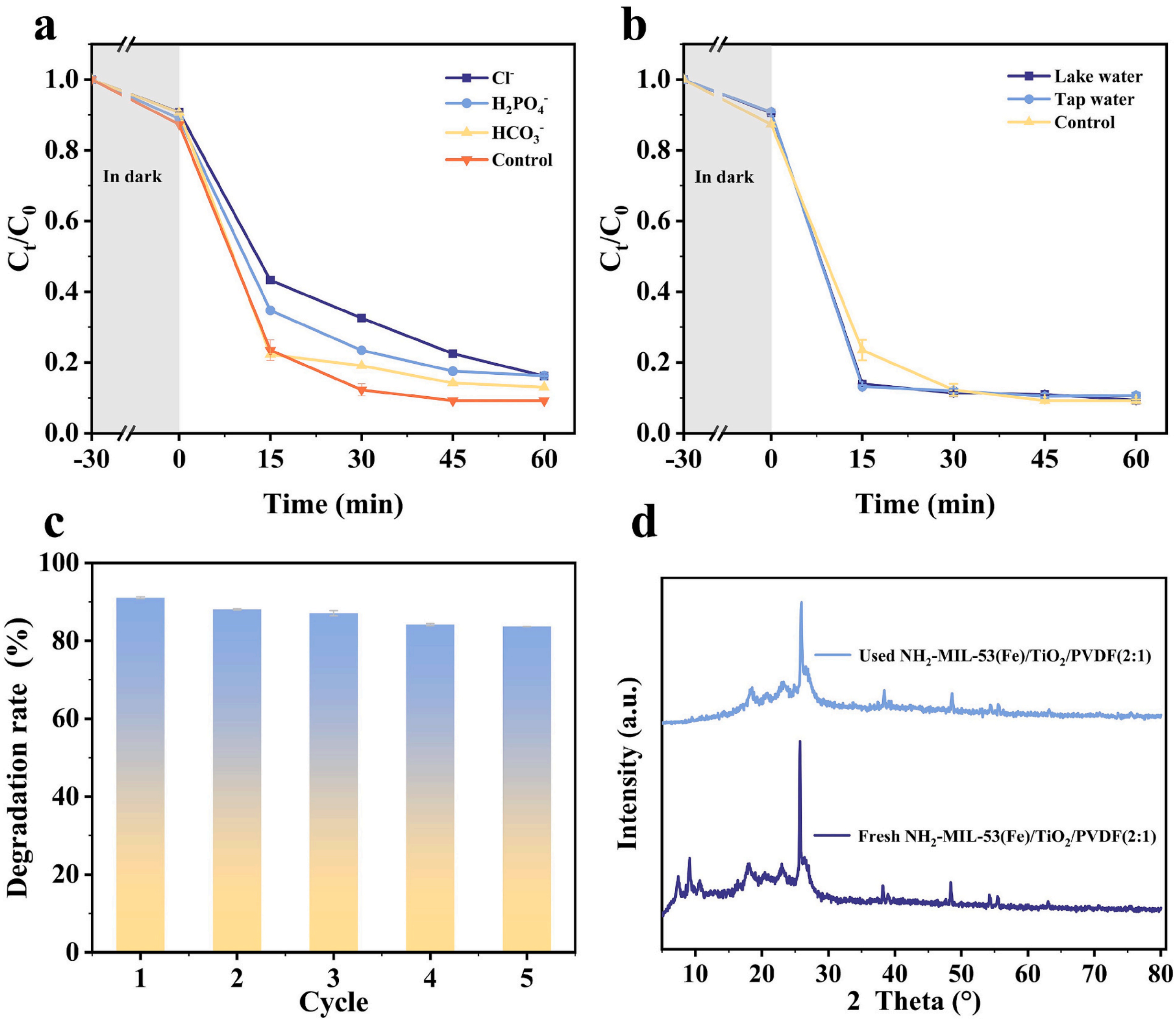

Fig. 7. (a) The influence of different inorganic anions on the photo-Fenton degradation of TC in NH_2-MIL-53(Fe)/TiO_2/PVDF membrane (b) Photo-Fenton degradation of TC in actual water samples (c) TC degradation cycle experiment (d) XRD patterns of NH_2-MIL-53(Fe)/TiO_2/PVDF membrane before and after recycling test.

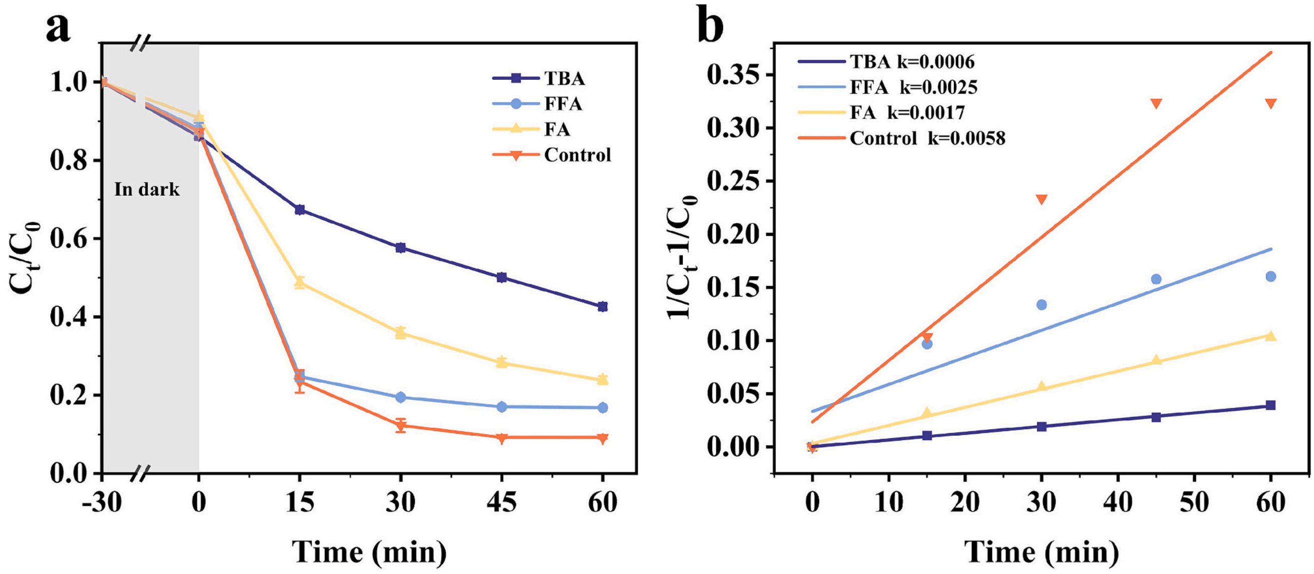

Fig. 8. (a) Effect of different scavengers on photo-Fenton degradation of TC and (b) the corresponding second-order kinetic fitting curves.

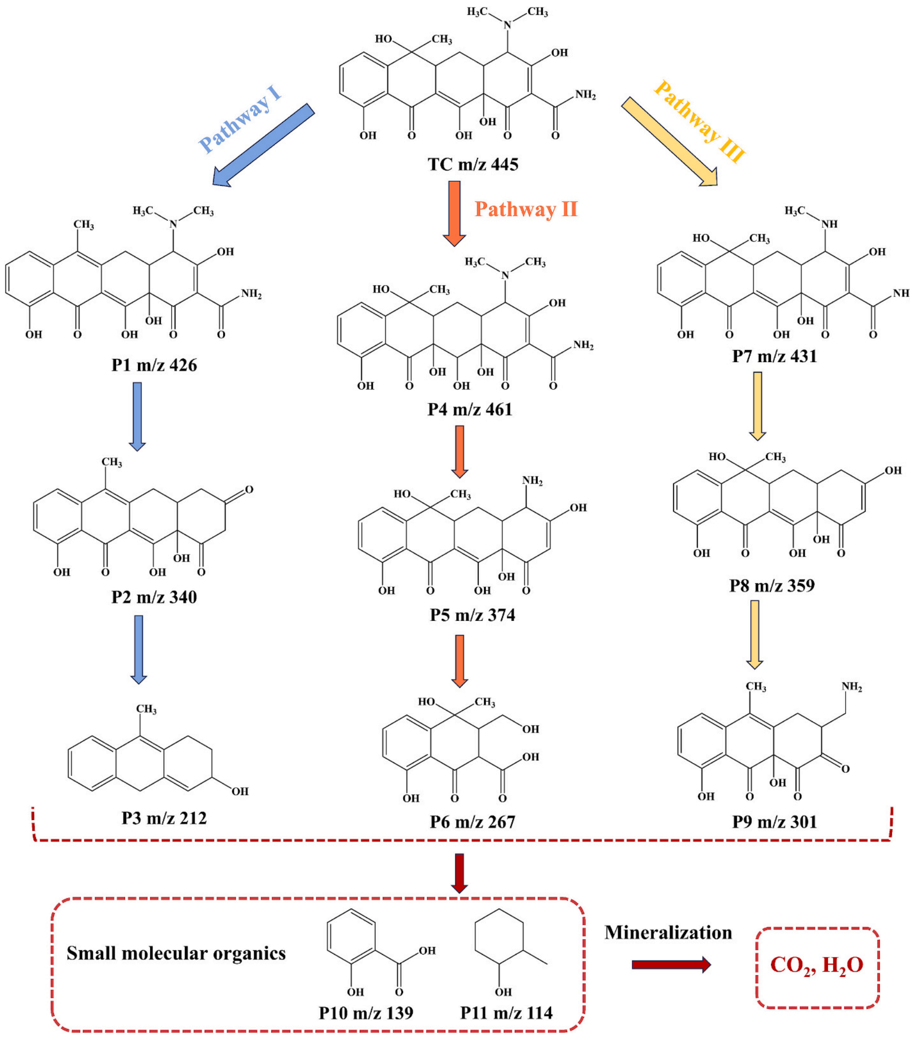

Fig. 9. The degradation pathway of TC.

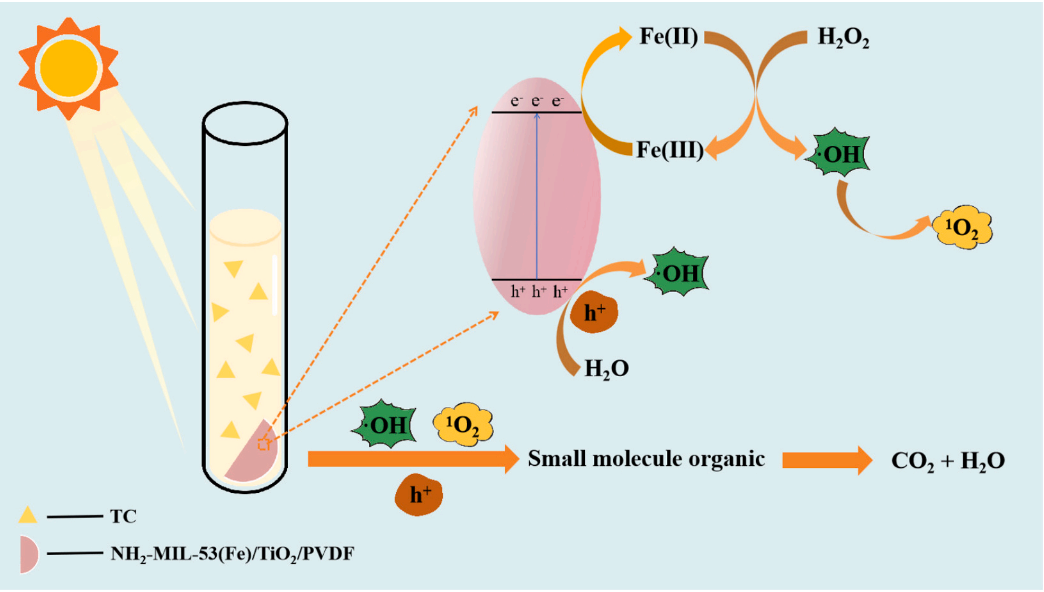

Fig. 10. The mechanism for degradation of TC.

pathways for TC. Pathway I: TC ($m/z = 445$) was firstly degraded by dehydration to P1 ($m/z = 426$), which was subsequently degraded to P2 ($m/z = 340$) by hydroxylated amide, and P2 by further dihydroxylation, dealkylation and ring-opening reactions resulting in the formation of P3 ($m/z = 212$). Pathway II: TC ($m/z = 445$) polymerized via double bond addition to form hydroxylated P4 ($m/z = 461$), P4 was converted by demethylation, deamidation, and dihydroxylation to form P5 ($m/z = 374$), P5 underwent ring-opening reaction and amino oxidation, leading to the further production of P6 ($m/z = 267$). Pathway III: TC ($m/z = 445$) was first degraded to P7 ($m/z = 431$) by dealkylation reaction, P7 formed P8 ($m/z = 359$) by *N*-demethylation and deamidation, P8 further generated P9 ($m/z = 301$) through dihydroxylation and ring-opening reactions. Subsequently, as a result of the continuous attack of the active species, some intermediate molecular products were further formed, including P10 ($m/z = 139$) and P11 ($m/z = 114$), which were ultimately mineralized into CO_2 and H_2O [49–54].

3.3.3. TC degradation mechanism in the NH_2-MIL-53(Fe)/TiO_2/PVDF + H_2O_2 + light system

Following the aforementioned analyses, a potential mechanism for TC degradation was suggested (Fig. 10). Firstly, NH_2-MIL-53(Fe)/TiO_2/PVDF membrane, serving as a photocatalyst, generated e^- and h^+ when exposed to visible light (Eq. 2). One part of h^+ migrates to the surface of the catalyst for the direct degradation of TC, and the other part of h^+ forms ·OH by oxidizing H_2O (Eq. 3) [55]. Secondly, photogenerated electrons (e^-) within the photo-Fenton reaction are capable of reducing Fe(III) to Fe(II) (Eq. 4). The Fe(III)/Fe(II) active center within NH_2-MIL-53(Fe)/TiO_2/PVDF reacts with H_2O_2 to form ·OH (Eq. 5) and mildly oxidized ·OOH (Eq. 6). In addition, ·OH further generates $^1O_2$ (Eq. 7), and TC is degraded into small-molecule organic compounds by ·OH, h^+, and $^1O_2$, and finally into CO_2 and H_2O (Eq. 8) [56,57].

$$NH_2-MIL-53(Fe)/TiO_2/PVDF + h\nu \rightarrow e^- + h^+ \tag{2}$$

$$h^+ + H_2O \rightarrow \cdot OH + H^+ \tag{3}$$

$$Fe(III) + e^- \rightarrow Fe(II) \tag{4}$$

$$Fe(II) + H_2O_2 \rightarrow Fe(III) + \cdot OH + OH^- \tag{5}$$

$$Fe(III) + H_2O_2 \rightarrow Fe(II) + \cdot OOH + H^+ \tag{6}$$

$$4\cdot OH \rightarrow {}^1O_2 + 2H_2O \tag{7}$$

$$\cdot OH/{}^1O_2\Big/h^+ + TC \rightarrow \text{Small molecule organic} \rightarrow CO_2 + H_2O \tag{8}$$

4. Conclusion

In summary, NH_2-MIL-53(Fe)/TiO_2/PVDF was prepared by vacuum filtration as a photocatalytic membrane for TC degradation. The simultaneous introduction of NH_2-MIL-53(Fe) and TiO_2 conferred upon the membrane a highly efficient photo-Fenton catalytic activity for the degradation of TC. Due to the synergistic effect of H_2O_2, visible light and catalyst, the best degradation performance of TC was achieved under the photo-Fenton reaction system. In addition, NH_2-MIL-53(Fe)/TiO_2/PVDF photocatalytic membrane exhibited satisfactory recyclability and stability after five cycles. Furthermore, loading the catalyst onto the membrane not only facilitated recycling of catalyst but also mitigated pollution resulting from direct addition. The free radical trapping experiments showed that ·OH was the main active species in the degradation of TC. According to MS results, TC formed eleven possible degradation intermediate products through three degradation pathways. This study provides valuable reference for the rapid recovery of catalysts in heterogeneous photo-Fenton systems.

CRediT authorship contribution statement

Jia-Xin Song: Writing – original draft, Visualization, Methodology, Investigation, Formal analysis. **Lei-Qin Sun:** Validation, Methodology, Investigation, Formal analysis. **Shu-Ting Cheng:** Investigation, Formal analysis. **Xiao-Fang Shen:** Methodology, Investigation, Formal analysis. **Yue-Hong Pang:** Writing – review & editing, Resources, Project administration, Funding acquisition.

Declaration of competing interest

The authors declare that they have no known competing financial interests or personal relationships that could have appeared to influence the work reported in this paper.

Acknowledgments

This work was supported by the National Natural Science Foundation of China (22276077).

Appendix A. Supplementary data

Supplementary data to this article can be found online at https://doi.org/10.1016/j.jwpe.2025.106943.

Data availability

Data will be made available on request.

References

[1] Y.J. Ben, C.X. Fu, M. Hu, L. Liu, M.H. Wong, C.M. Zheng, Human health risk assessment of antibiotic resistance associated with antibiotic residues in the environment: a review, Environ. Res. 169 (2019) 483–493, https://doi.org/10.1016/j.envres.2018.11.040.

[2] C.H. Liu, H.L. Dai, C.Q. Tan, Q. Pan, F. Hu, X. Peng, Photo-Fenton degradation of tetracycline over Z-scheme Fe-g-C_3N_4/Bi_2WO_6 heterojunctions: mechanism insight, degradation pathways and DFT calculation, Appl. Catal. B Environ. 310 (2022) 121326, https://doi.org/10.1016/j.apcatb.2022.121326.

[3] Y.H. Xue, J.J. Wang, M. Wang, J. Li, K.F. Wang, A. Hassan, C.Y. Guo, J.D. Wang, Magnetic porous material derived from Ni-MOF for the removal of tetracycline from aqueous solution, ACS Appl. Nano Mater. (2024), https://doi.org/10.1021/acsanm.4c00278.

[4] M.F. Cui, Y.H. Li, Y. Sun, H.M. Wang, M.X. Li, L.B. Li, W.S. Xu, Degradation of tetracycline in polluted wastewater by persulfate over copper alginate/graphene oxide composites, J. Polym. Environ. 29 (2021) 2227–2235, https://doi.org/10.1007/s10924-020-02038-6.

[5] N. Hanna, P. Sun, Q. Sun, X. Li, X. Yang, X. Ji, H. Zou, J. Ottoson, L.E. Nilsson, B. Berglund, O.J. Dyar, A.J. Tamhankar, C. Stålsby Lundborg, Presence of antibiotic residues in various environmental compartments of Shandong province in eastern China: its potential for resistance development and ecological and human risk, Environ. Int. 114 (2018) 131–142, https://doi.org/10.1016/j.envint.2018.02.003.

[6] Yu Q.S., Ding M.J., Wei Z.Q., Zhao J.W., Zhang H.N, 2024. Photoelectrochemical studies of Sn doped FeOCl and photo-Fenton degradation of tetracycline. J. Solid State Chem. 337, 124816. doi:https://doi.org/10.1016/j.jssc.2024.124816.

[7] Yu Q.S., Ding M.J., Wei Z.Q., Zhao J.W., Zhang H.N, 2024. Ginkgo biloba-derived biochar loaded with FeOCl for photo-Fenton degradation of tetracycline. Mater. Sci. Semicond. Process. 184, 108790. doi:https://doi.org/10.1016/j.mssp.2024.108790.

[8] Yao X.W., Cheng Z.K., Agathokleous E., Wei Y.Q., Feng X.Y., Li H.H., Zhang T.T., Li S.T., Dhawan G., Luo X.S, 2024. Tetracycline and sulfadiazine toxicity in human liver cells Huh-7. Environ. Pollut. 345, 123454. doi:https://doi.org/10.1016/j.envpol.2024.123454.

[9] D. Liu, L.L. Lu, M. Wang, B. Hussain, S. Tian, W.J. Luo, J.L. Zhou, X.E. Yang, Tetracycline uptake by pak choi grown on contaminated soils and its toxicity in human liver cell line HL-7702, Environ. Pollut. 253 (2019) 312–321, https://doi.org/10.1016/j.envpol.2019.06.086.

[10] G.H. Du, Y. Yang, L. Tian, X. Chen, Y. Zhang, J. Zhao, F. Luo, S. Shan, T. Hu, Y. He, Fabrication of Fe-based biomass aerogel with microwave assistance and its properties in the removal of tetracycline from wastewater, J. Environ. Chem. Eng. 12 (2024) 112343, https://doi.org/10.1016/j.jece.2024.112343.

[11] R. Gusain, K. Gupta, P. Joshi, O.P. Khatri, Adsorptive removal and photocatalytic degradation of organic pollutants using metal oxides and their composites: a comprehensive review, Adv. Colloid Interf. Sci. 272 (2019) 102009, https://doi.org/10.1016/j.cis.2019.102009.

[12] A. Saravanan, P.S. Kumar, R.V. Hemavathy, S. Jeevanantham, M.J. Jawahar, J. P. Neshaanthini, R. Saravanan, A review on synthesis methods and recent applications of nanomaterial in wastewater treatment: challenges and future perspectives, Chemosphere 307 (2022) 135713, https://doi.org/10.1016/j.chemosphere.2022.135713.

[13] Z.B. Wang, H.B. Wang, P. Wang, X. Liu, X. Lei, R. Guo, J. You, H. Zhang, Application of MOFs driven by various energy sources for degradation the organic pollutants in water: a review, Coord. Chem. Rev. 499 (2024) 215506, https://doi.org/10.1016/j.ccr.2023.215506.

[14] M.N. Liu, L. Zhang, M.H. Wang, X. Wang, H. Cui, J. Wei, X. Li, The role of metal-organic frameworks in removing emerging contaminants in wastewater, J. Clean. Prod. 429 (2023) 139526, https://doi.org/10.1016/j.jclepro.2023.139526.

[15] J.F. Bao, S.S. Guo, D.D. Fan, J. Cheng, Y. Zhang, X. Pang, Sonoactivated nanomaterials: a potent armament for wastewater treatment, Ultrason. Sonochem. 99 (2023) 106569, https://doi.org/10.1016/j.ultsonch.2023.106569.

[16] A. Hassani, M. Malhotra, A.V. Karim, S. Krishnan, P.V. Nidheesh, Recent progress on ultrasound-assisted electrochemical processes: a review on mechanism, reactor strategies, and applications for wastewater treatment, Environ. Res. 205 (2022) 112463, https://doi.org/10.1016/j.envres.2021.112463.

[17] Q.S. Wu, M.S. Siddique, Y.L. Guo, M. Wu, Y. Yang, H. Yang, Low-crystalline bimetallic metal-organic frameworks as an excellent platform for photo-Fenton degradation of organic contaminants: intensified synergism between hetero-metal nodes, Appl. Catal. B Environ. 286 (2021) 119950, https://doi.org/10.1016/j.apcatb.2021.119950.

[18] Zhang, M.H., Dong, H., Zhao, L., Wang, D.-x., Meng, D., 2019. A review on Fenton process for organic wastewater treatment based on optimization perspective. Sci. Total Environ. 670, 110–121. doi:https://doi.org/10.1016/j.scitotenv.2019.03.180.

[19] Y.P. Zhu, R.L. Zhu, Y.F. Xi, J. Zhu, G. Zhu, H. He, Strategies for enhancing the heterogeneous Fenton catalytic reactivity: a review, Appl. Catal. B Environ. 255 (2019) 117739, https://doi.org/10.1016/j.apcatb.2019.05.041.

[20] N. Thomas, D.D. Dionysiou, S.C. Pillai, Heterogeneous Fenton catalysts: a review of recent advances, J. Hazard. Mater. 404 (2021) 124082, https://doi.org/10.1016/j.jhazmat.2020.124082.

[21] Q.S. Wu, M.S. Siddique, H.J. Wang, L. Cui, H. Wang, M. Pan, J. Yan, Visible-light-driven iron-based heterogeneous photo-Fenton catalysts for wastewater decontamination: a review of recent advances, Chemosphere 313 (2023) 137509, https://doi.org/10.1016/j.chemosphere.2022.137509.

[22] M.I. Irfan, M. Sadiq, L. Zohra, A.B. Siddique, M. Yousaf, M. Rubab, K. Urooj, A. Aziz, H. Ali, M. Fatima, H.M.A. Amin, H.A. Alhazmi, A. Abbas, Chemical modification of Pinus walliichiana sawdust: application in membrane system for efficient purification of groundwater containing cd(II) and Ni(II), J. Water Process Eng. 68 (2024) 106337, https://doi.org/10.1016/j.jwpe.2024.106337.

[23] N.F. Atta, H.M.A. Amin, M.W. Khalil, A. Galal, Nanotube arrays as Photoanodes for dye sensitized solar cells using metal Phthalocyanine dyes, Int. J. Electrochem. Sci. 6 (8) (2011) 3316–3332, https://doi.org/10.1016/S1452-3981(23)18254-X.

[24] A.W. Khan, N.S. Lali, F.Y. Sabei, M.I. Irfan, M. Naeem-ul-Hassan, M. Sher, A. Y. Safhi, A. Alsalhi, A.H. Albariqi, F. Kamli, H.M.A. Amin, A. Abbas, Sunlight-assisted green synthesis of gold nanocubes using horsetail leaf extract: a highly selective colorimetric sensor for Pb^{2+}, photocatalytic and antimicrobial agent, J. Environ. Chem. Eng. 12 (3) (2024) 112576, https://doi.org/10.1016/j.jece.2024.112576.

[25] A. Shah, S. Akhtar, F. Mahmood, S. Urooj, A.B. Siddique, M.I. Irfan, M. Naeem-ul-Hassan, M. Sher, A. Alhoshani, A. Rauf, H.M.A. Amin, A. Abbas, Fagonia arabica extract-stabilized gold nanoparticles as a highly selective colorimetric nanoprobe for Cd^{2+} detection and as a potential photocatalytic and antibacterial agent, Surfaces Interfaces 51 (2024) 104556, https://doi.org/10.1016/j.surfin.2024.104556.

[26] J.J. Li, J.H. You, Z.W. Wang, Y. Zhao, J. Xu, X. Li, H. Zhang, Application of α-Fe_2O_3-based heterogeneous photo-Fenton catalyst in wastewater treatment: a review of recent advances, J. Environ. Chem. Eng. 10 (2022) 108329, https://doi.org/10.1016/j.jece.2022.108329.

[27] S.Z. Yang, X. Li, G.M. Zeng, M. Cheng, D. Huang, Y. Liu, C. Zhou, W. Xiong, Y. Yang, W. Wang, G. Zhang, Materials institute Lavoisier (MIL) based materials for photocatalytic applications, Coord. Chem. Rev. 438 (2021) 213874, https://doi.org/10.1016/j.ccr.2021.213874.

[28] B. Kaur, V. Soni, R. Kumar, P. Singh, R. Selvasembian, A. Singh, S. Thakur, A. Khan, S. Kaya, L. Nguyen, V. Nguyen, P. Raizada, Recent advances in manipulating strategies of NH_2-functionalized metallic organic frameworks-based heterojunction photocatalysts for the sustainable mitigation of various pollutants, Environ. Res. 259 (2024) 119575, https://doi.org/10.1016/j.envres.2024.119575.

[29] Y.Y. Li, Y. Fang, Z.L. Cao, N. Li, D. Chen, Q. Xu, J. Lu, Construction of g-C_3N_4/PDI@MOF heterojunctions for the highly efficient visible light-driven degradation of pharmaceutical and phenolic micropollutants, Appl. Catal. B Environ. 250 (2019) 150–162, https://doi.org/10.1016/j.apcatb.2019.03.024.

[30] Q.Y. Zhang, W.G. Xu, L.P. Wang, J. Song, X. Xu, Fabrication of boron nitride decorated NH_2-MIL-53(Fe) for efficient removal of typical antibiotics, Opt. Mater. 142 (2023) 114092, https://doi.org/10.1016/j.optmat.2023.114092.

[31] Y.C. Xie, J.Q. Wan, Z.C. Yan, Y. Wang, T. Xiao, J. Hou, H. Chen, Targeted degradation of sulfamethoxazole in wastewater by molecularly imprinted MOFs in advanced oxidation processes: degradation pathways and mechanism, Chem. Eng. J. 429 (2022) 132237, https://doi.org/10.1016/j.cej.2021.132237.

[32] Shahzad, R., Muneer, M., Khalid, R., Amin, H.M.A, 2023. ZnO-Bi_2O_3 heterostructured composite for the photocatalytic degradation of orange 16 reactive dye: synergistic effect of UV irradiation and hydrogen peroxide. Catalysts. 2023; 13(10):1328. doi:https://doi.org/10.3390/catal13101328.

[33] F. Nada, Galal A. Atta, H.M.A. Amin, Synthesis and photoelectrochemical behavior of a hybrid electrode composed of polyaniline encapsulated in highly ordered TiO_2 nanotubes array, Int. J. Electrochem. Sci. 7 (4) (2012) 3610–3626, https://doi.org/10.1016/S1452-3981(23)13982-4.

[34] S.A.G. Krishnan, B. Sasikumar, G. Arthanareeswaran, Z. László, E. Nascimben Santos, G. Veréb, S. Kertész, Surface-initiated polymerization of PVDF membrane using amine and bismuth tungstate (BWO) modified MIL-100(Fe) nanofillers for pesticide photodegradation, Chemosphere 304 (2022) 135286, https://doi.org/10.1016/j.chemosphere.2022.135286.

[35] J.J. Xue, M.J. Xu, J.M. Gao, Y. Zong, M. Wang, S. Ma, Multifunctional porphyrinic Zr-MOF composite membrane for high-performance oil-in-water separation and organic dye adsorption/photocatalysis, Colloids Surf. A Physicochem. Eng. Asp. 628 (2021) 127288, https://doi.org/10.1016/j.colsurfa.2021.127288.

[36] L.-Q. Sun, X.-F. Shen, H.-M. Zhang, Y.-H. Pang, Amino-functionalized iron-based MOFs for rhodamine B degradation in heterogeneous photo-Fenton system, J. Photochem. Photobiol. A Chem. 452 (2024) 115544, https://doi.org/10.1016/j.jphotochem.2024.115544.

[37] J.H. Huang, J.L. Hu, Y.H. Shi, G. Zeng, W. Cheng, H. Yu, Y. Gu, L. Shi, K. Yi, Evaluation of self-cleaning and photocatalytic properties of modified g-C_3N_4 based PVDF membranes driven by visible light, J. Colloid Interface Sci. 541 (2019) 356–366, https://doi.org/10.1016/j.jcis.2019.01.105.

[38] C. Wang, Y.L. Wu, J. Lu, J. Zhao, J.Y. Cui, X.L. Wu, Y.S. Yan, P.W. Huo, Bioinspired synthesis of photocatalytic nanocomposite membranes based on synergy of Au-TiO_2 and polydopamine for degradation of tetracycline under visible light, ACS Appl. Mater. Interfaces 9 (2017) 23687–23697, https://doi.org/10.1021/acsami.7b04902.

[39] K.J. Zhang, Y.J. Fu, D. Hao, J. Guo, B.-J. Ni, B. Jiang, L. Xu, Q. Wang, Fabrication of CN75/NH_2-MIL-53(Fe) p-n heterojunction with wide spectral response for efficiently photocatalytic Cr(VI) reduction, J. Alloys Compd. 891 (2022) 161994, https://doi.org/10.1016/j.jallcom.2021.161994.

[40] J.A. Borrego-Pérez, F. González, C.A. Meza-Avendaño, I.M. De Los Santos, R. López-Juárez, I. Hernández, E.M. Alonso-Guzman, W. Martinez-Molina, H. L. Chavez-Garcia, Structural, optical and photoluminescence properties of TiO_2 and TiO_2: Tm^{3+} nanopowders, Optik 227 (2021) 166083, https://doi.org/10.1016/j.ijleo.2020.166083.

[41] W.P. Xiong, Z.T. Zeng, X. Li, G. Zeng, R. Xiao, Z.H. Yang, Y. Zhou, C. Zhang, M. Cheng, L. Hu, C. Zhou, L. Qin, R. Xu, Y. Zhang, Multi-walled carbon nanotube/amino-functionalized MIL-53(Fe) composites: remarkable adsorptive removal of antibiotics from aqueous solutions, Chemosphere 210 (2018) 1061–1069, https://doi.org/10.1016/j.chemosphere.2018.07.084.

[42] P.F. Sun, X. Zhang, Z.R. Guo, X. Liu, Y. Lan, D. Zhang, H. Li, J. Li, H. Liu, X. Xu, An adsorptive photo-Fenton-like removal of 1,2-benzisothiazolin-3-one by NH2-MIL-53(Fe) under simulated solar light, New J. Chem. 47 (17) (2023) 8334–8346, https://doi.org/10.1039/D3NJ00771E.

[43] R.B. Guo, W.J. Qin, B.J. Wang, L. Li, Q. Chen, Y. Tan, Y. Zhong, Z. Zhao, N. Liu, Z. Mo, NH2-MIL-88B(Fe)/TiO2/PAN electrostatically spun nanofiber membrane for photocatalytic degradation of tetracycline and oil-water separation, Sep. Purif. Technol. 351 (2024) 128059, https://doi.org/10.1016/j.seppur.2024.128059.

[44] Y.J. Gou, P. Chen, L. Yang, S. Li, L. Peng, S. Song, Y. Xu, Degradation of fluoroquinolones in homogeneous and heterogeneous photo-Fenton processes: a review, Chemosphere 270 (2021) 129481, https://doi.org/10.1016/j.chemosphere.2020.129481.

[45] Y.B. Zhao, L. Chang, Y.Y. Li, W. He, K. Liu, M. Cui, M.U. Hameed, J. Xie, High-gravity photocatalytic degradation of tetracycline hydrochloride under simulated sunlight, J. Water Process Eng. 53 (2023) 103753, https://doi.org/10.1016/j.jwpe.2023.103753.

[46] J. Hang, X.H. Yi, C.C. Wang, H. Fu, P. Wang, Y. Zhao, Heterogeneous photo-Fenton degradation toward sulfonamide matrix over magnetic Fe_3S_4 derived from MIL-100 (Fe), J. Hazard. Mater. 424 (2022) 127415, https://doi.org/10.1016/j.jhazmat.2021.127415.

[47] C.Y. Yang, Z.H. Zhang, P. Wang, P. Xu, T. Shen, M. Wang, Q. Zheng, G. Zhang, Ultrathin g-C_3N_4 composite Bi_2WO_6 embedded in PVDF UF membrane with enhanced permeability, anti-fouling performance and durability for efficient removal of atrazine, J. Hazard. Mater. 451 (2023) 131154, https://doi.org/10.1016/j.jhazmat.2023.131154.

[48] C. Gao, S. Chen, X. Quan, H. Yu, Y. Zhang, Enhanced Fenton-like catalysis by iron-based metal organic frameworks for degradation of organic pollutants, J. Catal. 356 (2017) 125–132, https://doi.org/10.1016/j.jcat.2017.09.015.

[49] Z. Cao, Y. Zhao, Z. Zhou, Q. Wang, Q. Mei, H. Cheng, Efficiency $LaFeO_3$ and BiOI heterojunction for the enhanced photo-Fenton degradation of tetracycline hydrochloride, Appl. Surf. Sci. 590 (2022) 153081, https://doi.org/10.1016/j.apsusc.2022.153081.

[50] X. Li, X. Shen, Y. Qiu, Z. Zhu, H. Zhang, D. Yin, Fe_3O_4 quantum dots mediated P-g-C_3N_4/BiOI as an efficient and recyclable Z-scheme photo-Fenton catalyst for tetracycline degradation and bacterial inactivation, J. Hazard. Mater. 456 (2023) 131677, https://doi.org/10.1016/j.jhazmat.2023.131677.

[51] X. Li, X. Zhang, S. Wang, P. Yu, Y. Xu, Y. Sun, Highly enhanced heterogeneous photo-Fenton process for tetracycline degradation by Fe/SCN Fenton-like catalyst, J. Environ. Manag. 312 (2022) 114856, https://doi.org/10.1016/j.jenvman.2022.114856.

[52] X. Wang, X. Lin, X. Wu, I. Lynch, Z-scheme Fe@Fe_2O_3/BiOBr heterojunction with efficient carrier separation for enhanced heterogeneous photo-Fenton activity of tetracycline degradation: Fe^{2+} regeneration, mechanism insight and toxicity evaluation, Environ. Res. 252 (2024) 118396, https://doi.org/10.1016/j.envres.2024.118396.

[53] G. Yang, Y. Liang, Z. Xiong, J. Yang, K. Wang, Z. Zeng, Molten salt-assisted synthesis of Ce_4O_7/Bi_4MoO_9 heterojunction photocatalysts for photo-Fenton degradation of tetracycline: enhanced mechanism, degradation pathway and products toxicity assessment, Chem. Eng. J. 425 (2021) 130689, https://doi.org/10.1016/j.cej.2021.130689.

[54] X. Zhang, B. Ren, X. Li, B. Liu, S. Wang, P. Yu, Y. Xu, G. Jiang, High-efficiency removal of tetracycline by carbon-bridge-doped g-C_3N_4/Fe_3O_4 magnetic heterogeneous catalyst through photo-Fenton process, J. Hazard. Mater. 418 (2021) 126333, https://doi.org/10.1016/j.jhazmat.2021.126333.

[55] J.Y. Zheng, C. Liu, Z.W. Wang, Y. Shi, Y. Hou, J. Bi, L. Wu, Improving photocatalytic degradation of enrofloxacin over TiO_2 nanosheets with Ti^{3+} sites by coordination activation, Appl. Catal. A Gen. 660 (2023) 119217, https://doi.org/10.1016/j.apcata.2023.119217.

[56] Z.M. Fang, Y.B. Liu, J.J. Qi, Z.-F. Xu, T. Qi, L. Wang, Establishing a high-speed electron transfer channel via CuS/MIL-Fe heterojunction catalyst for photo-Fenton degradation of acetaminophen, Appl. Catal. B Environ. 320 (2023) 121979, https://doi.org/10.1016/j.apcatb.2022.121979.

[57] J.Y. Zhang, M.W. Yan, G.C. Sun, X. Li, B. Hao, K. Liu, Mg–Fe–Al–O spinel: preparation and application as a heterogeneous photo-Fenton catalyst for degrading rhodamine B, Chemosphere 304 (2022) 135318, https://doi.org/10.1016/j.chemosphere.2022.135318.